BIOSCIENCE JOURNAL

# SPATIAL PATTERNS OF MORTALITY FROM RESPIRATORY DISEASES AND THEIR RELATIONSHIP WITH SOCIO-ENVIRONMENTAL INDICATORS IN BRAZIL

Nícholas de Paula NICOMEDES[1], Pedro Cesar Madureira de Godoy CAMARGO[2], Luis Armando de Oro ARENAS[3], Liliane Moreira NERY[1], Leopoldo André Dutra LUSQUINO-FILHO[2], Darllan Collins da Cunha e SILVA[3]

[1]Postgraduate Program in Environmental Sciences, Institute of Science and Technology, Universidade Estadual Paulista, Sorocaba, São Paulo State, Brazil.
[2]Department of Control and Automation Engineering, Institute of Science and Technology, Universidade Estadual Paulista, Sorocaba, São Paulo State, Brazil.
[3]Department of Environmental Engineering, Institute of Science and Technology, Universidade Estadual Paulista, Sorocaba, São Paulo State, Brazil.

**How to cite:** NICOMEDES, N.P., et al. Spatial patterns of mortality from respiratory diseases and their relationship with socio-environmental indicators in Brazil. *Bioscience Journal*. 2026, **42**, e42012. https://doi.org/10.14393/BJ-v42n0a2026-78449



**Abstract**

This study analyzes the spatial autocorrelation of mortality rates from respiratory diseases in Brazilian municipalities between 1999 and 2022, emphasizing associated socioeconomic and environmental factors, including GDP per capita, population density, urbanization index, and greenhouse gas (GHG) emissions. Statistical analyses related to the Global Moran's I and Local Moran's Index (LISA) were applied to identify spatial patterns of dependence, followed by Pearson correlation analysis. The results reveal a reduction in the global autocorrelation of mortality over time, with persistent high-risk clusters in the South and Southeast regions, especially among the elderly and groups with higher education levels, while the North and Northeast regions show greater vulnerability associated with low education, income, and urbanization. GHG emissions maintained distinct spatial patterns over the period, with $CH_4$ showing relative stability, whereas $CO_2$ and $N_2O$ showed an increase in spatial autocorrelation in more recent years. The findings reinforce the importance of spatial analysis in identifying territorial health inequalities and provide support for integrated public policies aligned with the Sustainable Development Goals (SDGs) aimed at mitigating the effects of climate change and promoting socio-environmental equity.

**Keywords:** Air pollution. Climate change. Public health. Social vulnerability. Spatiotemporal autocorrelation. Spatial epidemiology.

**Corresponding author:**
Nícholas de Paula Nicomedes
nicholas.nicomedes@unesp.br

**Received:** 05 June 2025
**Accepted:** 08 April 2026
**Published:** 24 April 2026

## 1. Introduction

Climate change has intensified extreme events and altered global climate patterns, directly impacting human health. Rising average temperatures, the increased frequency and intensity of heatwaves, droughts, and air pollution represent significant challenges for public health systems across the world. In Europe, Ayres et al. (2009) highlighted the impacts of climate change on respiratory diseases, while in Africa, McCutcheon, Vachiat, and Manga (2022) reported that rising average temperatures and extreme events are associated with worsening cardiovascular disease.

The Intergovernmental Panel on Climate Change (IPCC 2023) report emphasizes that exposure to extreme climate conditions is associated with increased mortality from cardiovascular and respiratory diseases, especially among vulnerable populations. Moreover, socioeconomic factors play a key role in determining the population's susceptibility to these diseases, influencing access to health services, the quality of the urban environment, and exposure to air pollutants (Nichols et al. 2018; McCutcheon et al. 2022).

In Brazil, socioeconomic and regional disparities exacerbate the impacts of climate change on public health. Previous studies indicate that the spatial distribution of respiratory diseases is associated with urbanization, air pollution, and socioeconomic vulnerability (Confalonieri and Marinho 2007; Silva et al. 2014).

Air pollution has been identified as one of the leading causes of worsening respiratory diseases, especially in densely populated metropolitan regions (Ayres et al. 2009). At the same time, sociodemographic characteristics, such as race, education level, and age, stand out in the distribution of mortality from respiratory diseases, reflecting structural inequalities in access to healthcare and exposure to environmental risk factors (Baqui et al. 2021; Anunciação et al. 2022). Despite this evidence, the literature still lacks comprehensive studies evaluating the spatial distribution of respiratory mortality in Brazil and its temporal correlation with climate and socioeconomic indicators.

Therefore, this study aims to provide support for the formulation of more effective public policies to mitigate the impacts of climate change on health, in line with the United Nations Sustainable Development Goals (SDGs), particularly those related to public health (SDG 3) and climate action (SDG 13) (UN 2015).

In this context, this study analyzes the spatial distribution of mortality rates from respiratory diseases across Brazilian municipalities from 1999 to 2022. It aims to identify spatial autocorrelation patterns using Global Moran's I and the Local Moran's Index (LISA). Additionally, it investigates the correlation between general and classified mortality, by education level, age group, race, and sex, correlates with socioeconomic and environmental variables such as GDP per capita, population density, urbanization index, and GHG emissions

## 2. Material and Methods

### Dataset organization

*Mortality data collection and crude rate calculation*

Mortality information was obtained from the DATASUS TABNET system, based on vital statistics classified according to the 10th Revision of the International Statistical Classification of Diseases and Related Health Problems (ICD-10), in accordance with the World Health Organization (WHO) standards. Annual data were collected for all Brazilian municipalities from 1999 to 2022, focusing on Respiratory Diseases (ICD-10: J00–J99).

A database was structured with variables classified by education level, age group, race, and sex. Education was divided into three levels: no formal education, 1 to 11 years, and 12 years or more. The age group was organized into five categories: age group of 1 year, 1 to 14 years, 15 to 39 years, 40 to 59 years, and 60 years or older. The racial categories were yellow, white, indigenous, brown, and black. Sex was classified as female or male.

According to Equation 1, crude mortality rates were calculated per 100,000 inhabitants to reduce distortions caused by small population sizes in municipalities (Silva et al. 2014, Gomes et al. 2025). The

calculation was performed using an algorithm written in *Python*, applied to the total number of cases and defined population categories, allowing integration into Geographic Information Systems (GIS).

$$\text{Mortality Rate}_{year} = \frac{n_{dth}}{P_{mun}} \times 100.000 \quad (1)$$

Where:
$n_{dth}$: number of deaths;
$P_{mun}$: population of the municipality.

*Collection of socioeconomic data*

Population data, per capita Gross Domestic Product (GDP) values, and municipal boundaries were obtained from the Brazilian Institute of Geography and Statistics (IBGE) for the period 1999 to 2022. During data organization, gaps were identified in the demographic and economic information for newly emancipated municipalities, with some data unavailable in certain years. To correct these inconsistencies, official municipal emancipation and installation dates were consulted, and territorial meshes and corresponding data were adjusted according to each municipality's administrative validity.

Municipal population estimates were used for intercensal years, while census data were maintained for 2000, 2010, and 2022. For municipalities without recorded demographic data, the IBGE (2011) estimation methodology was adopted, based on proportionality and correction coefficients, as shown in Equations 2 to 5.

$$P(t) = \sum_{i=1}^{n} P_i(t) \quad (2)$$

$$P_i(t) = a_i P(t) + b_i \quad (3)$$

$$a_i = \frac{P_i(t_1) - P_i(t_0)}{P(t_1) - P(t_0)} \quad (4)$$

$$b_i = P_i(t_0) - a_i P(t_0) \quad (5)$$

Where:
P: Population of the federative unit;
$P_i$: Population of municipality *i*;
$a_i$: Proportionality coefficient of population growth;
$b_i$: Linear correction coefficient;
t: Year being calculated;
$t_0$: Census 1;
$t_1$: Census 2.

The urbanization index was obtained from the Land Use and Land Cover (LULC) database provided by the MapBiomas Brazil project. The variable was derived from the ratio of urbanized area to total municipal area.

During data extraction, we identified omission errors where the automated MapBiomas classification returned to zero urban area for certain small municipalities. To fill these specific gaps, we did not employ automated classification algorithms but rather conducted a visual interpretation and manual vectorization of the urban footprint using historical Landsat 7 multispectral imagery (30-meter resolution). Because this study relies on a long historical time series (1999–2022), retrospective in-situ ground truth validation and the calculation of traditional accuracy metrics (e.g., error matrices) were unfeasible.

In specific cases, such as the archipelago of Fernando de Noronha, which MapBiomas does not classify, historical high-resolution imagery from Google Earth Pro was utilized. A visual temporal analysis confirmed that urban expansion in this municipality remained highly stable throughout the analyzed period.

This stability is consistent with its geographical isolation as an island and its strict legal designation as an environmental conservation unit, which severely limits land use and occupation.

*Environmental data collection*

Information on atmospheric emissions associated with climate change was obtained from the EDGAR - Emission Database for Global Atmospheric Research platform, which provides annual inventories of anthropogenic GHG emissions derived from globally consistent, model-based approaches (Crippa et al. 2024). The EDGARv8.0 (2023) database, developed in collaboration between the Joint Research Centre (JRC) and the International Energy Agency (IEA), was used, focusing on the standardization and consistency of emission estimates from fossil fuel combustion.

The three main GHGs were considered: carbon dioxide ($CO_2$), methane ($CH_4$), and nitrous oxide ($N_2O$). The original EDGAR data are provided at a spatial resolution of 0.1° × 0.1° (Crippa et al., 2024), which is coarser than many Brazilian municipalities. This scale mismatch results in spatial discretization effects, where multiple municipalities may share identical emission values from a single grid cell, thereby limiting the representation of intra-regional variability and hindering the adaptation of gridded emission inventories to local scales (Edebeli et al. 2021).

To address this limitation, a spatial resampling procedure was applied using the Inverse Distance Weighted (IDW) method, generating continuous emission surfaces at a finer spatial resolution (0.01° × 0.01°; ~1136.9 m). It is important to emphasize that this procedure does not aim to increase the intrinsic accuracy of the EDGAR data, but rather to improve spatial compatibility between emission data and municipal boundaries for subsequent aggregation.

The finer spatial resolution allows a more consistent allocation of emission values within municipal polygons, increasing the number of raster cells intersecting each municipality and reducing artifacts associated with coarse grid aggregation. Similar approaches for the spatial analysis of emissions at finer scales have been reported in the literature (Ye et al. 2025).

Municipal average emissions were then calculated using zonal statistics, considering the overlap of municipal polygons on the interpolated rasters. To standardize spatial comparisons, the original values were converted to gas tons per square kilometer per year (t/km²/year), allowing more accurate and comparable analyses of emission intensities across Brazilian municipalities.

**Spatial analytical structure**

*Assessment of global spatial autocorrelation*

Spatial autocorrelation of mortality rates began with the Global Moran's I assessment, applied to total deaths and to categories classified by education level, age group, race, and sex. The analysis was conducted in ArcMap 10.8 using the Spatial Autocorrelation (Moran's I) tool.

The Global Moran's I calculation was based on a municipality contiguity matrix, following the principles established by Câmara et al. (2004), ensuring topological consistency. Municipalities without spatial contiguity - such as Ilha Bela and Fernando de Noronha - were excluded from the analysis due to the impossibility of calculating the index arising from their geographic isolation.

For each analyzed year, the following parameters were extracted: the observed Global Moran's I value, the expected value, the variance, the z-score, and the p-value, with a significance level of 0.05. The results were organized into time series and summarized using descriptive statistical indices, including minimum, maximum, mean, and standard deviation.

*Identification of local clusters*

Based on the Global Moran's I results, the years in which each mortality rate - total and by subgroups - presented extreme values (maximum and minimum) of spatial autocorrelation were selected. These years were analyzed in greater detail using LISA to identify significant spatial clusters at the municipal level.

The analysis was conducted in ArcMap 10.8 using the Cluster and Outlier Analysis (Anselin Local Moran's I) tool. The neighborhood matrix was constructed based on edge contiguity, and statistical significance was assessed using a pseudo-significance test with 9,999 permutations.

Municipalities classified with significant spatial autocorrelation in High-High (HH) and Low-Low (LL) clusters were selected. These municipalities were organized into an integrated database to investigate correlation patterns with socioeconomic and environmental variables. For this stage, mortality rates with significant autocorrelation were overlaid independently of the analysis category (general or by class). This increased analysis accuracy and reduced potential biases related to variable selection or spatial noise.

**Data processing, normalization, and variable analysis**

Data processing was carried out in the Jupyter Notebook environment, with the analytical workflow structured into organized stages. The datasets were loaded and stored in Python dictionary structures, allowing efficient access to Data Frames and facilitating operations such as table joins, time series extraction, and variable type handling.

To allow comparisons among variables with different scales, z-score normalization was applied, as shown in Equation 6, transforming variables with different scales into a common distribution and ensuring their comparability.

$$x_i^* = \frac{(x_i - \mu_x)}{\sigma_x} \quad (6)$$

Where:
$x_i$: original value of the variable;
$\mu_x$: mean value of the variable;
$\sigma_x$: standard deviation of the variable.

The Combined Variable was constructed using Equation 7, a composite metric obtained by summing the socioeconomic and environmental variables (GHG emissions, urbanization index, population density, and GDP per capita) from the normalized variables.

$$\text{Combined}_{\text{Variable}_i} = \sum_j x_i^{*(j)} \quad (7)$$

Where:
$x_i^{*(j)}$: normalized variable *j* for municipality *i*.

The choice of an additive combination aimed to ensure that each variable contributes proportionally to the unimodal variable (Combined Variable), preserving comparability and avoiding scale bias. This synthetic metric enables the joint evaluation of multiple socioeconomic and environmental factors about mortality, facilitating the identification of aggregated patterns and complex interactions.

Although creating unimodal variables can accentuate multicollinearity in some contexts, prior standardization mitigates this risk by equalizing the magnitudes of the variables. The adopted approach preserves the statistical structure of the original variables while reducing the problem's dimensionality.

The next step involved calculating Pearson correlation coefficients, applied annually for each municipality, as presented in Equation 8. This technique assessed linear relationships between mortality rates and socioeconomic and environmental variables, including the composite variable. Records with missing or inconsistent data were previously removed to ensure the robustness of the analyses.

$$p_{x,y} = \frac{\text{Cov}(x,y)}{\sigma x, \ \sigma y} \quad (8)$$

Where:
*Cov* (x,y): covariance between variables x and y;
σ: standard deviation of each variable.

The choice of an unweighted additive combination aimed to ensure that each normalized variable contributes equally to the composite metric, preserving comparability and avoiding scale bias. While we acknowledge that an unweighted sum ignores empirical weighting, this method was deliberately chosen to retain the interpretability of the original factors without introducing arbitrary or subjective weights into the model.

It is important to emphasize that this Combined Variable serves as a complementary, exploratory macro-metric. The core robust interpretations of our study are based on the isolated variables. However, this synthetic metric provides a comprehensive measure of the overall socio-environmental exposure, facilitating the identification of aggregated spatial patterns that might not be immediately evident in individual analyses. Although constructing a composite metric can sometimes exacerbate multicollinearity, prior z-score standardization mitigates this risk by equalizing magnitudes and preventing any single variable from dominating the index. This approach ensures a transparent synthesis of complex interactions while reducing the problem's dimensionality for exploratory visualization.

Finally, to account for spatial autocorrelation and prevent biased estimates inherent to traditional OLS models, we expanded our analytical framework beyond exploratory Pearson correlations by implementing spatial econometrics. Specifically, a Spatial Error Model (SEM) was applied to the municipal data (Anselin 1988; LeSage and Pace 2009). The SEM incorporates a spatial weights matrix (contiguity-based) to capture the spatial dependence in the error term, controlled by the parameter ($\lambda$). The choice of the SEM specification was supported by spatial diagnostics of the OLS residuals, which indicated significant spatial clustering in the unmodeled errors.

**Spatial representation of results**

Correlation visualization was carried out using heatmaps generated with the Seaborn library in the Python environment. In conventional charts, rows correspond to mortality profiles by category, while columns represent the socioeconomic and environmental variables analyzed.

The layout was inverted for the representations associated with the Combined Variable: the row represents the unimodal variable, and the columns correspond to the different mortality categories. This approach provided a clear visualization of the intensity and direction of the correlations, allowing for the identification of recurring patterns and relevant relationships between social and environmental determinants and the different mortality classes.

Additionally, for the variables with the most expressive Pearson correlation coefficients, positive and negative, choropleth maps were generated to spatially represent the distribution of these correlations at the municipal level. These maps enabled the identification of areas where the relationships between explanatory factors and mortality from respiratory diseases showed the most excellent spatial consistency, highlighting the territorial variation of the identified statistical associations.

## 3. Results

**Spatial autocorrelation of mortality rates**

The global spatial autocorrelation analysis for general mortality from respiratory diseases revealed a decreasing trend in Global Moran's I values over the analyzed period. The mean Global Moran's I value was 0.33, with the highest value observed in 1999 (0.43) and the lowest in 2007 (0.15), as shown in Figure 1.

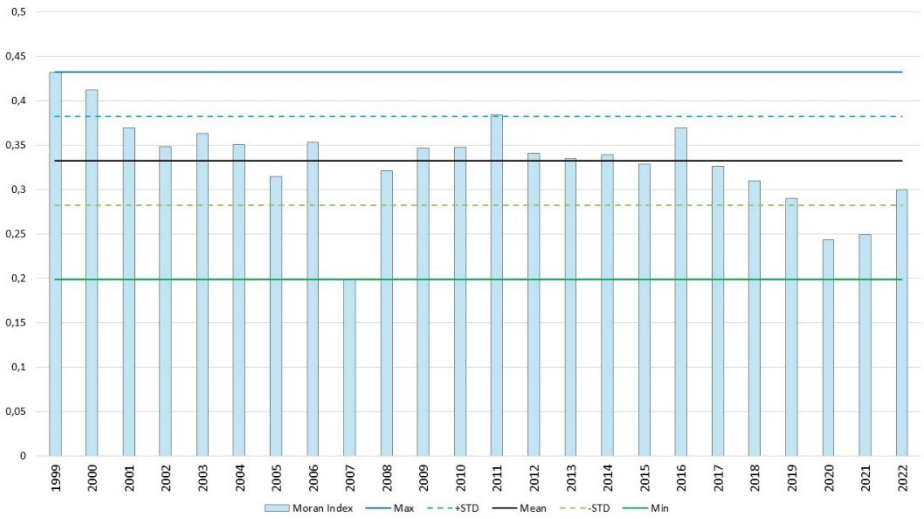


**Figure 1**. Global Moran's I for mortality from respiratory system diseases.
Legenda: +STD – Mean plus standard deviation; −STD – Mean minus standard deviation.

The results stratified by education level indicated that groups with 1 to 11 years of education (E1) had the highest spatial autocorrelation values throughout the period (Figure 2a). Regarding age group (Figure 2b), higher spatial autocorrelation was found in older groups, especially among populations aged 60 or older (AG5). This pattern indicates that deaths from respiratory diseases tend to be spatially concentrated among the elderly population.


**Figure 2.** Global Moran's I for mortality from respiratory system diseases by (A) education level, (B) age group, (C) race, and (D) sex.
Legend: E0 – No formal education; E1 – 1 to 11 years of education; E2 – 12 years or more of education; AG1 – Age group under 1 year; AG2 – Age group 1 to 14 years; AG3 – Age group 15 to 39 years; AG4 – Age group 40 to 59 years; AG5 – Age group 60 years or older; YE – Yellow; WH – White; IN – Indigenous; BW – Brown; BK – Black; F– Female; M – Male.

Regarding race (Figure 2c), a significant temporal variation in Global Moran's I values was observed, with increased autocorrelation among the brown population in recent years. In general, the highest values were recorded among the white and brown populations. Finally, Global Moran's I values by sex (Figure 2d) indicated that, until 2020, men had higher spatial autocorrelation in mortality rates. From 2011 onwards, however, a significant increase in autocorrelation among women was observed, reducing the gap between the sexes.

## Spatial autocorrelation of socioeconomic and environmental variables

The spatial autocorrelation assessment of socioeconomic variables showed distinct Global Moran's I patterns. GDP per capita (Figure 3a) had a mean value of 0.31, while population density (Figure 3c) had a mean of 0.45, both showing temporal variation without a clear trend of increase or decrease. On the other hand, the urbanization index (Figure 3b) remained more stable and began to grow in 2010, reaching a mean of 0.48.

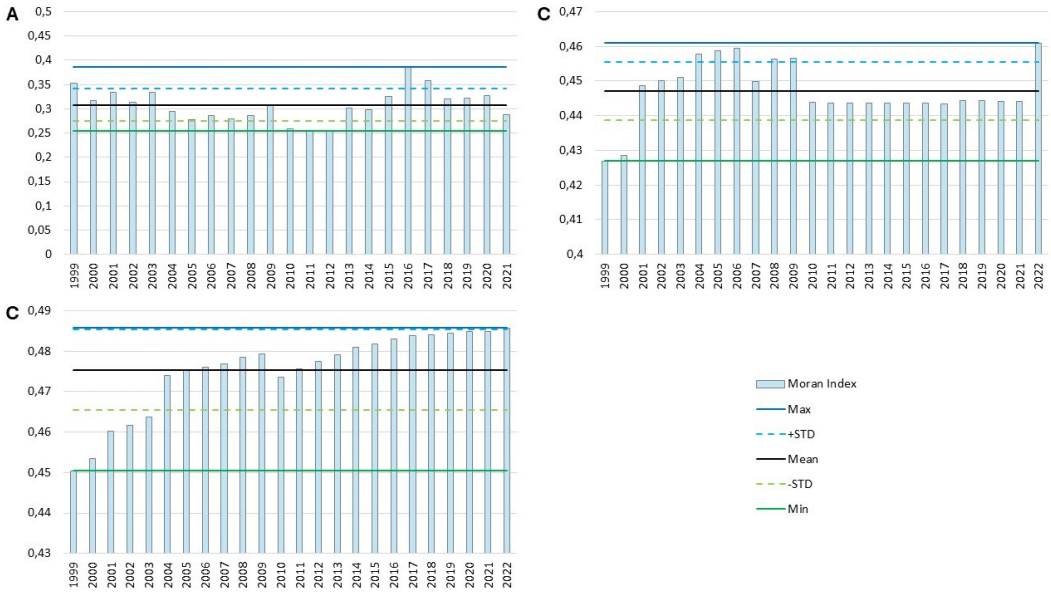


**Figure 3**. Global Moran's I for (A) GDP per capita, (B) population density, and (C) urbanization index.
Legenda: +STD – Mean plus standard deviation; −STD – Mean minus standard deviation.

Regarding variables associated with climate change, Global Moran's I values varied for GHG emissions, with average spatial dependence for the three analyzed gases. $CH_4$ had a mean value of 0.29 (Figure 4a), $CO_2$ had the highest mean value, at 0.51 (Figure 4b), and $N_2O$ reached 0.47 (Figure 4c). These results indicate strong spatial aggregation of emissions, especially for $CO_2$.

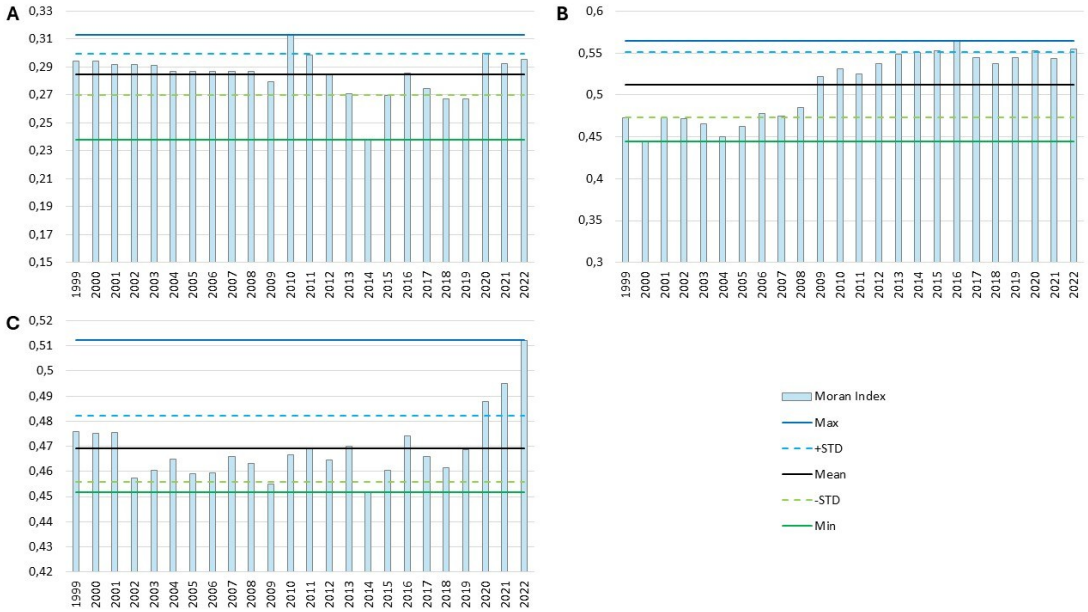


**Figure 4.** Global Moran's I for (A) $CH_4$ concentration, (B) $CO_2$ concentration, and (C) $N_2O$ concentration.
Legenda: +STD – Mean plus standard deviation; −STD – Mean minus standard deviation.

The $CH_4$ Global Moran's I time series remained consistently stable, with a peak in 2010. For $CO_2$ and $N_2O$, the indices showed growth in recent years, with $CO_2$ increasing from 2009 onward and $N_2O$ from 2020, reaching the highest spatial autocorrelation in 2022.

**Identification of spatial mortality clusters**

Significant spatial clusters were identified using LISA, applied exclusively to the years with extreme (maximum and minimum) Global Moran's I values for each dependent variable (Table 1). The spatial distribution of the identified clusters is available in an interactive WebGIS environment (Supplementary material).

**Table 1**. Years of highest and lowest Global Moran's I for each dependent variable analyzed.

| Variable | Class | Year of Highest GISA | Year of Lowest GISA |
|---|---|---|---|
| General mortality | Mortality | 1999 | 2007 |
| Mortality – Age Group | AG1 | 2014 | 2018 |
| | AG2 | 2008 | 2017 |
| | AG3 | 1999 | 2011 |
| | AG4 | 1999 | 2019 |
| | AG5 | 1999 | 2007 |
| Mortality – Sex | M | 1999 | 2021 |
| | F | 2016 | 2004 |
| Mortality – Education | E0 | 2022 | 2005 |
| | E1 | 1999 | 2007 |
| | E2 | 2015 | 2005 |
| Mortality – Race | YE | 1999 | 2002 |
| | WH | 2016 | 2007 |
| | IN | 2004 | 2005 |
| | BW | 2022 | 1999 |
| | BK | 2020 | 2006 |

Legend: E0 – No formal education; E1 – 1 to 11 years of education; E2 – 12 years or more of education; AG1 – Age group under 1 year; AG2 – Age group 1 to 14 years; AG3 – Age group 15 to 39 years; AG4 – Age group 40 to 59 years; AG5 – Age group 60 years or older; YE – Yellow; WH – White; IN – Indigenous; BW – Brown; BK – Black; F– Female; M – Male.

For general mortality, the LISA spatial patterns in 1999 showed a predominance of Low-Low (LL) clusters in the North and Northeast and High-High (HH) clusters in the South and Southeast. In 2007, these clusters were redistributed, with HH clusters forming in Ceará and Pernambuco and intensifying the pattern in Rio Grande do Sul.

For populations aged 60 or older (AG5), the typical distribution of HH in the South and Southeast and LL in the North and Northeast remained in both analyzed years (1999 and 2007). For the 40-59 age group (AG4), LL clusters were observed in states such as Amazonas, Pará, Maranhão, and Tocantins, with reduced HH clusters in 2019 and increased dispersion in the Center-West. For ages 15–39 (AG3) and 1-14 (AG2), patterns were mostly not significant, with a few municipalities classified as HH or LL distributed at random. Children under 1-year-old (AG1) showed HH concentration in Amazonas, Pará, Maranhão, and Mato Grosso do Sul in 2014 and 2018.

The analysis by education level showed that, among groups with no formal education (E0), HH clusters formed in Ceará, Rio Grande do Norte, Pernambuco, and Minas Gerais in 2022, whereas in 2005 these municipalities were predominantly LL or not significant. In the same period, São Paulo and Santa Catarina showed LL concentrations. Among those with 1 to 11 years of education (E1), HH patterns predominated in the South and Southeast in 1999, with LL clusters expanding in the North in 2007. For groups with 12 or more years of education (E2), HH clusters were concentrated in SP, RJ, and southern MG (2015 and 2005), while LL clusters were absent in both years.

Regarding sex, for men, the HH pattern persisted in the South and Southeast and, in 2021, also in the Center-West. The LL pattern was constant in the North and Northeast in both years analyzed (1999 and 2021). For women, in 2016, HH clusters were observed in the Center-West, South, and Southeast, particularly in Rio

Grande do Sul, while LL clusters predominated in the North, Bahia, and Piauí. In 2004, HH clusters were less expressive and more dispersed.

Finally, for race, spatial cluster distribution showed varied patterns. For the black population, LL areas were concentrated in Pará, Amazonas, Santa Catarina, and Paraná, while HH clusters were located in Rio de Janeiro, Minas Gerais, Maranhão, Tocantins, Piauí, and Bahia. Among the brown population, in 1999, LL clusters were in the South, while HH clusters appeared in the Center-West, Southeast, and Northeast; in 2022, LL regions predominated in SP, MG, and the South, with HH clusters in the Northeast. For the white population, HH clusters remained in the Southeast and South (2001 and 2007), while LL clusters were in the North and Northeast.

Among the yellow population, only a few municipalities in MG and CE reported HH in 1999; in 2020, the pattern was mostly not significant. For the Indigenous population, HH clusters and transition zones (low-high) were observed in the North and Center-West in 2022, especially in AM, RR, PA, MT, MS, and AC. In 1999, only 20 municipalities were classified as HH, and most areas remained insignificant in both years.

Thus, the LISA spatial cluster analysis enabled classification of municipalities into HH and LL groups.

**Statistical correlations between explanatory variables and mortality**

Only municipalities with statistically significant HH or LL spatial autocorrelation for general and classified mortality rates, as identified in the LISA analysis, were considered. In total, 5,028 municipalities met this criterion, which is shown in green in Figure 5, while the remaining 542 municipalities with no significant autocorrelation are highlighted in red.

This study is a subsequent phase of a broader project titled "*Spatial correlation analysis by deep learning of morbidity and mortality rates with indicators associated with climate and socioeconomic changes*" (complete data available at: https://app.powerbi.com/view?r=eyJrIjoiYWI3MmVkMTktMDE3ZC00ZWEzLTg4MzEtMzkwZTlhYzhlMjRjIiwidCI6ImZlODc4N2JjLWM5MTQtNDY2NS04NTQ3LTI2OGUxNWNiMGQ5YSJ9).

Within this main project, the filtering approach was deliberately chosen to ensure that statistical correlations were evaluated only for locations with consolidated spatial patterns of high or low risk. By removing non-significant and transitional areas (Low-High or High-Low Autocorrelation), we avoided introducing spatial noise that could bias the relationships between health variables and socio-environmental indicators. Since the 5,028 selected municipalities represent approximately 90% of the Brazilian territory, this approach maintains robust national representativeness.

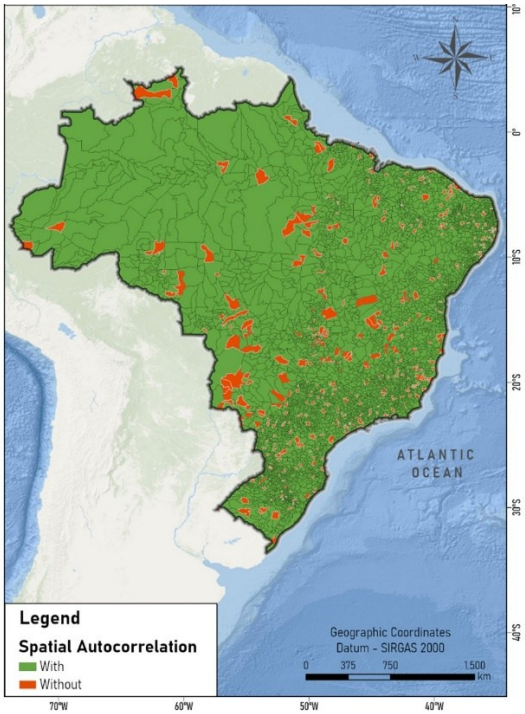


**Figure 5**. Spatial autocorrelation of Brazilian municipalities for diseases associated with climate change.

The Pearson correlations between explanatory variables, both socioeconomic and environmental, and mortality rates showed different patterns across the analyzed categories, presented in Figure 6. Regarding race, mortality rates among the brown population at the municipal level showed the strongest negative correlation with GDP per capita (-0.29), indicating an inverse relationship between socioeconomic level and mortality. On the other hand, the white population at the municipal level showed the highest positive correlation (0.30), indicating a direct association between higher income and higher recorded mortality. We hypothesize that this counterintuitive pattern may be related to better case detection and reporting in wealthier regions, a premise further explored in the Discussion.


**Figure 6**. Pearson correlation heatmap between respiratory disease mortality rates by class and independent variables.

Legend: RT – Rate; E0 – No formal education; E1 – 1 to 11 years of education; E2 – 12 or more years of education; AG1 – Age group under 1 year; AG2 – Age group 1 to 14 years; AG3 – Age group 15 to 39 years; AG4 – Age group 40 to 59 years; AG5 – Age group 60 years or older; YE – Yellow; WH – White; IN – Indigenous; BW – Brown; BK – Black; F – Female; M – Male; CH4 – Methane; CO2 – Carbon dioxide; N2O – Nitrous oxide.

The white and yellow populations showed positive correlations with all explanatory variables, especially nitrous oxide ($N_2O$), with values of 0.19 for whites and 0.14 for yellows. The indigenous population showed predominantly negative correlations, indicating inverse relationships with socio-environmental factors.

Regarding education, classes with some level of education (E1 and E2) showed positive correlations with all variables, with the highest correlation between E2 and urbanization index (0.3), while population with no formal education (E0) showed a positive correlation only with $N_2O$ and a negative correlation with other indicators. The highest positive correlation observed was between groups with 1 to 11 years of education (E1 and E2) and GDP per capita (0.29), while the absence of education was negatively correlated with the urbanization index (-0.15).

Sex-based analyses indicated that both men and women had positive correlations with socioeconomic and environmental indicators, although values were higher for males. The highest correlation was between men and GDP per capita (0.22), while correlations for women, though positive, were lower.

In terms of age group, younger groups (under 14 years) showed negative correlations with all variables, with the highest negative values observed for ages 1 to 14 (-0.14 with GDP per capita) and under 1 year (-0.13 with GDP per capita). From age 40 onwards, correlations became predominantly positive, with the 60+ group having the highest correlation with GDP per capita (0.21).

In the analysis of the Combined Variable, illustrated in Figure 7, the results showed positive correlations with the white population (0.13), those with up to 11 years of education (0.15), those with 12 or more years of education (0.11), and people aged 60 or older (0.10).


**Figure 7**. Pearson correlation heatmap for the unimodal analysis of mortality from respiratory diseases.

Legend: RT – Rate; E0 – No formal education; E1 – 1 to 11 years of education; E2 – 12 or more years of education; AG1 – Age group under 1 year; AG2 – Age group 1 to 14 years; AG3 – Age group 15 to 39 years; AG4 – Age group 40 to 59 years; AG5 – Age group 60 years or older; M – Male; Combined – Combined variable.

The most expressive Pearson correlations were also spatialized through thematic maps, allowing the observation of territorial patterns of these associations. The relationship between GDP per capita and mortality of the white population (r = 0.30) was mainly positive across much of the country, especially in the Northeast, Southeast, Santa Catarina, and Paraná. However, the highest coefficients were concentrated in a few municipalities, as shown in Figure 8.

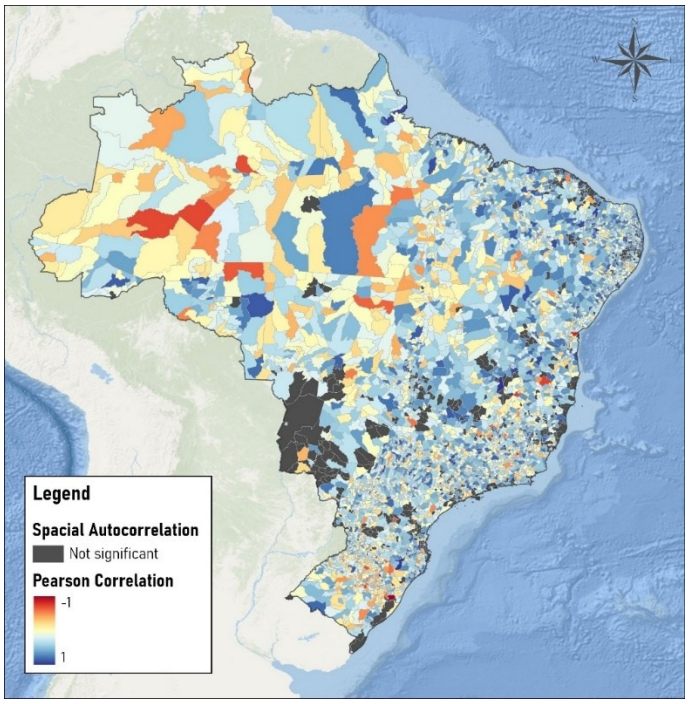


**Figure 8**. Thematic map of Pearson correlation between GDP per capita and respiratory disease mortality in the white population.

The correlation between GDP per capita and mortality in groups with 1 to 11 years of education (r = 0.29) was positive in most Brazilian municipalities, with notable exceptions in Rio Grande do Sul, such as Estrela and Rosário do Sul, which had significant negative values (Figure 9). The correlation between GDP per capita and brown population (r = -0.29) was positive in the Center-West, North, and South, especially in Santa Isabel do Rio Negro (AM) and Altamira (PA) (Figure 10).

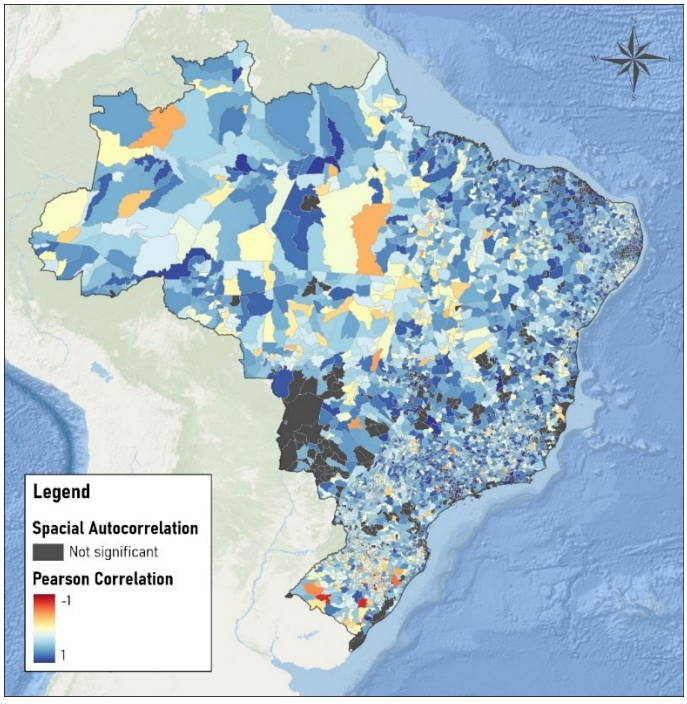


**Figure 9**. Thematic map of Pearson correlation between GDP per capita and respiratory disease mortality in groups with 1 to 11 years of education.

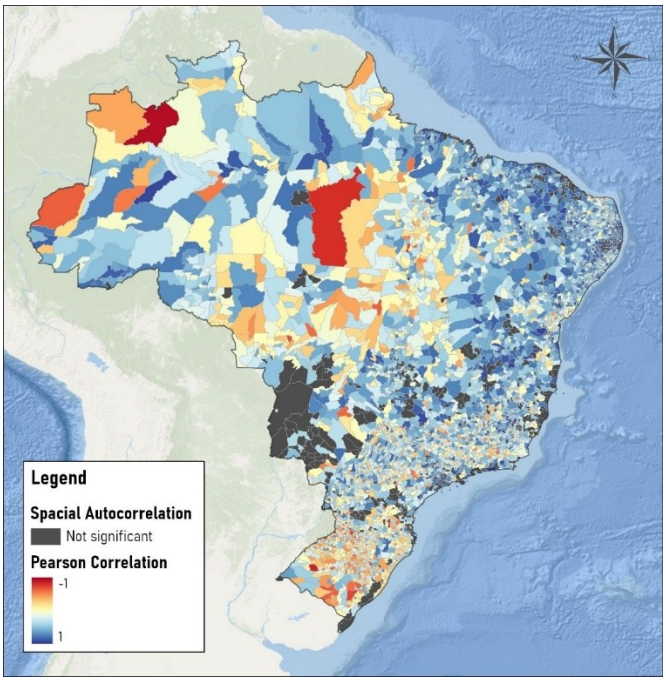


**Figure 10**. Thematic map of Pearson correlation between GDP per capita and respiratory disease mortality in the brown population.

Correlations between urbanization index and education level (E2) were predominantly negative (r = 0.30), with isolated positive values in the Southeast. This indicates important regional variations in the relationship between urbanization index and respiratory disease mortality among the more educated (Figure 11).

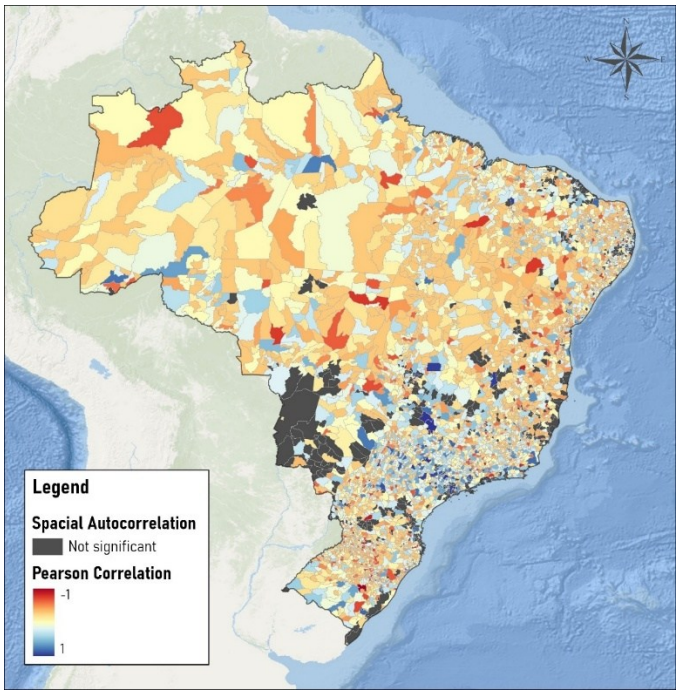


**Figure 11**. Thematic map of Pearson correlation between urbanization index and respiratory disease mortality in groups with 12 or more years of education.

Figure 12 presents the standardized beta coefficients derived from the SEM across all mortality profiles and socio-environmental predictors. By explicitly controlling spatial autocorrelation through the error term ($\lambda$), the SEM isolates the localized relationships, filtering out the inflationary effect of neighborhood spatial dependence.

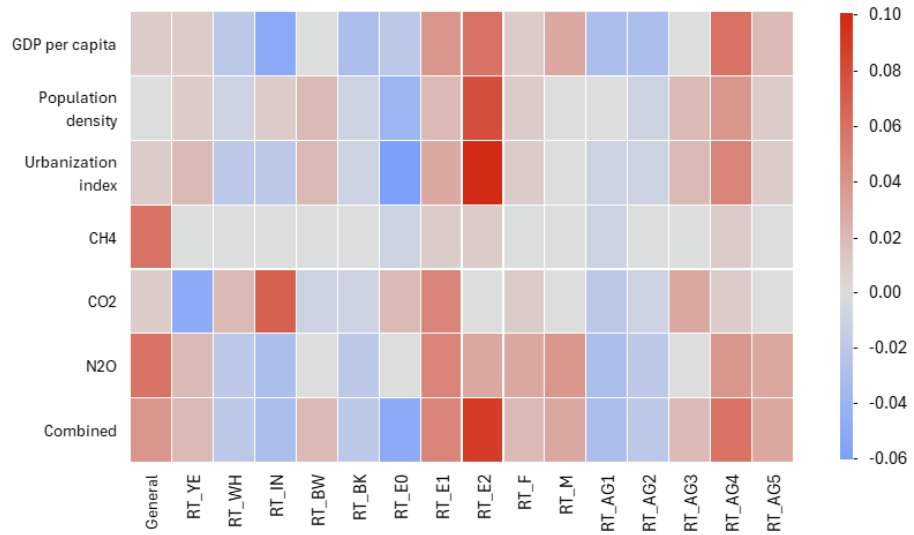


**Figure 12.** Spatial Error Model correlation heatmap between respiratory disease mortality rates by class, independent variables, and combined variable.

Legend: RT – Rate; E0 – No formal education; E1 – 1 to 11 years of education; E2 – 12 or more years of education; AG1 – Age group under 1 year; AG2 – Age group 1 to 14 years; AG3 – Age group 15 to 39 years; AG4 – Age group 40 to 59 years; AG5 – Age group 60 years or older; M – Male; Combined – Combined variable; General – General mortality.

Consequently, the standardized betas exhibit a more conservative, robust magnitude, ranging predominantly from -0.05 to +0.10. Analyzing the standardized SEM betas, the population with the highest educational attainment exhibited the strongest positive associations, particularly with the urbanization index (0.10) and the Combined Variable (0.09). Similarly, the adult population aged 40 to 59 years showed robust positive coefficients with GDP per capita (0.06) and the Combined Variable (0.06). Regarding environmental predictors, mortality within the yellow population showed distinct positive associations with municipal methane emissions (0.06) and nitrous oxide emissions (0.06).

Conversely, among the negative coefficients, inverse associations were most prominent in highly vulnerable demographic groups. Specifically, the population with no formal instruction showed a strong negative association with both the urbanization index (-0.06) and the Combined Variable (-0.05). Furthermore, a pronounced negative coefficient was identified between mortality in the brown population and municipal GDP per capita (-0.05). Detailed spatial diagnostics are available in the Supplementary Material.

## 4. Discussion

The analysis of Global Moran's I applied to mortality rates from respiratory diseases revealed a reduction in spatial autocorrelation over time, indicating a transition from highly concentrated patterns to a more diffuse distribution among municipalities. This trend may reflect improvements in the surveillance and control of these diseases and changes in the structural determinants of public health.

This behavior may be related to localized outbreaks in the late 1990s, which may have contributed to the increase in autocorrelation indices observed in 1999 (Nascimento et al. 2020). Additionally, factors such as increased tobacco consumption and inadequate diet may have contributed to occasional rises in mortality during that period.

The observed reduction in Global Moran's I values over the two decades coincides chronologically with the implementation of public health policies, such as the National Tobacco Control Program (PNCT), which contributed to a decline in smoking prevalence from 15.7% in 2006 to 9.8% in 2019 (Brazil 2021). While our ecological design precludes causal inference, we hypothesize that these national-level interventions reduced risk factors for chronic respiratory diseases (Cavalcante et al. 2017, Oliveira et al. 2022, Nery et al. 2026), thereby diluting highly concentrated severe case clusters.

The analysis by sex revealed a dynamic pattern. Men exhibited higher spatial autocorrelation until 2020, whereas from 2021 onwards, a significant increase in Global Moran's I values was observed among

women. This shift may be associated with intersectional factors, such as the unequal impacts of the COVID-19 pandemic. According to Razafindrakoto et al. (2021), Indigenous and Black women face elevated risks exacerbated by unfavorable socioeconomic conditions, low education levels, and limited access to healthcare, elements reflected in the observed spatial patterns.

LISA analyses reinforced the existence of persistent regional and demographic inequalities. The more urbanized and aged South and Southeast regions presented High-High (HH) spatial clusters, indicating a higher incidence of mortality from respiratory diseases. In contrast, HH clusters were more common among low-educated groups in the Northeast and Center-West, reflecting pronounced socioeconomic vulnerabilities.

Indigenous, Black, and brown populations concentrated HH clusters in historically marginalized areas, such as the Legal Amazon and the northeastern semi-arid region, whereas white and yellow populations exhibited such patterns in the South and Southeast regions with greater medical infrastructure and epidemiological surveillance (Anunciação et al. 2022).

These patterns highlight the urgency of public policies for equity in health, sanitation, education, and service access. The spatial analysis of variables enables visualization of how structural inequalities materialize territorially, directly impacting morbidity and mortality. The persistence of these clusters also suggests that recent social and economic transformations have not yet been sufficient to reverse such historical inequalities.

Positive correlations between education, GDP per capita, and urbanization index with mortality suggest that access to information, symptom recognition, and awareness of healthy lifestyle practices may influence the identification and management of these illnesses. Conversely, negative correlations indicate greater vulnerability in municipalities with populations of lower educational attainment, reflecting a lack of knowledge about health conditions and comorbidities and underreporting due to unawareness of risk factors (Baqui et al. 2021; Wetzel et al. 2023).

Limited access to health services, often associated with low education and distance from urban centers, hampers the search for medical guidance and regular examinations, contributing to the underreporting of health issues (Wetzel et al. 2023). This reality is particularly observed in Global South countries, such as Brazil, where regional and structural inequalities persist, especially in territories with a history of social exclusion. Neri and Soares (2002) indicate that groups in the lowest income deciles have worse access to health insurance, require more medical care, yet consume fewer health services. Additionally, Arruda et al. (2018) point to significant inequality in healthcare access between urban and rural areas, with lower access in rural areas due to greater social vulnerability and logistical difficulties.

To address these disparities, international cooperation initiatives have been implemented. In Brazil, an agreement with São Tomé and Príncipe was established to strengthen both countries' health systems, providing for partnerships in technical, technological, scientific, and human resources, as well as promoting human resource training, along with the international technical cooperation project “Support for the Tuberculosis Control Program of São Tomé and Príncipe,” which enabled infrastructure incorporation and training of health professionals (Brazil 2025). These actions exemplify how international cooperation, aligned with the SDGs - especially SDG 3 (Good Health and Well-Being) and SDG 10 (Reduced Inequalities) - can strengthen local health systems and promote greater equity in healthcare access.

Mortality showed positive correlations between older age groups and both GDP per capita and $N_2O$, highlighting age as a critical demographic factor. Populations in municipalities with a higher proportion of older age groups are more susceptible to severe aggregate outcomes from respiratory diseases (Baqui et al. 2021). The positive correlation with GDP per capita may reflect the location of this population in more economically developed regions with better access to healthcare.

Baqui et al. (2021) analyzed the COVID-19 context and identified geographic disparities in mortality. Wealthier areas had better health infrastructure and lower mortality rates, in contrast with poorer regions, which faced greater vulnerability.

The Brazilian urbanization process plays an ambivalent role among the structural determinants of health. While it increases access to infrastructure and medical services, it also intensifies territorial inequalities. Urban growth between 1985 and 2023 totaled 2.4 million hectares (MAPBIOMAS 2024), consolidating urban centers that concentrate 61% of the Brazilian population (IBGE 2022).

However, this process has historically been unequal. The national industrialization model concentrated investments in the Southeast and South regions, leaving the North and Northeast with lower economic and social development (Chaves 2020). These contrasts are reflected in the spatial mortality analyses and LISA patterns.

The spatial analysis of GHG emissions in Brazil reveals structural patterns strongly associated with land occupation and predominant economic activities. As Bustamante et al. (2012) point out, sectors such as agriculture and industry play a determining role in the spatial stability of these emissions, especially in the Amazon and Cerrado regions.

Livestock alone accounts for a significant share of national emissions, with variations ranging from 813 $MtCO_2eq$ to 1,090 $MtCO_2eq$ in pasture areas of these biomes between 2003 and 2008. The conversion of native vegetation for agricultural use, as observed in the Cerrado, has been identified as a relevant driver for increased nitrous oxide emissions (Locatteli et al. 2024).

The stability of carbon dioxide spatial patterns suggests that targets set by climate policies, such as Law No. 12.187/2009 (Brazil 2009) and Brazil's Nationally Determined Contributions (NDCs) under the Paris Agreement (Brazil 2023), have not yet produced significant effects on the territorial distribution of emissions. This finding reinforces the need for decentralized strategies tailored to regional specificities.

Beyond the spatial stability observed in emissions, the potential health effects must be interpreted within the broader epidemiological context. It is important to acknowledge the distinction between direct indoor toxicity and outdoor environmental exposure. The literature shows that high concentrations of GHGs have direct physiological impacts in controlled or occupational settings.

For instance, Satish et al. (2012) demonstrated cognitive impairment at $CO_2$ levels between 1,000 and 2,500 ppm, Kamens and Stern (1973) noted alterations in oxygenation from $CH_4$ above 10,000 ppm, and Menon et al. (2021) proposed strict occupational limits for $N_2O$ based on reproductive risks. However, as is frequently debated in environmental health, directly extrapolating these occupational thresholds to broad, open-air municipal settings poses significant limitations. While some models explore occupational limits to assess cumulative population risk (Dilger et al. 2022; Kleinbeck and Wolkoff 2024), outdoor GHG concentrations rarely reach these acute toxicity thresholds.

Therefore, for the scope of respiratory mortality in our ecological study, regions with high GHG emissions are best understood as robust indicators (proxies) of intense urbanization and the co-emission of air pollutants. As highlighted by Ayres et al. (2009) and the IPCC (2023), combined exposure to climate drivers and anthropogenic pollution poses a major challenge to respiratory health. Ultimately, the spatial autocorrelation of GHGs identified here highlights territories with severe environmental pollution, reflecting the structural vulnerabilities that drive respiratory mortality (Confalonieri and Marinho 2007).

The analysis of the Combined Variable revealed positive correlations with white groups, those with higher education, and groups aged 60 or older, indicating that mortality from respiratory diseases may be associated both with greater vulnerability among the elderly and greater case detection capacity in regions with better socioeconomic conditions (Gaffney et al. 2021; Du et al. 2023).

The spatialization of Pearson correlations revealed distinct territorial patterns. In the Southeast and South regions, positive correlations between explanatory variables and mortality predominated. Supported by the findings of Baqui et al. (2021), we hypothesize that this reflects better health surveillance infrastructure and greater access to precise diagnostics in these wealthier municipalities, rather than a strictly higher biological risk. In contrast, in the Center-West and Northeast, negative correlations predominated, suggesting that socially vulnerable populations face greater exposure to risks and barriers to healthcare access, leading to significant underreporting (Wetzel et al. 2023).

Although some patterns were consistent, the presence of weak correlations across much of the country highlights the complexity of the relationships between health and social, environmental, and economic determinants. This indicates that public policies should consider local specificities to ensure effective and equitable interventions.

The transition to the SEM framework confirmed that a significant portion of the variance captured by Pearson was indeed driven by neighborhood spillover effects, a common bias in aggregate ecological data where geographic boundaries do not contain socio-environmental dynamics (Anselin 2003). By controlling

this spatial noise within the error term, the standardized SEM betas yielded more conservative coefficients, effectively isolating the true local socio-environmental impacts.

Crucially, even after this rigorous spatial filtering, the core structural inequalities initially identified by the Pearson analysis remained robust. The SEM confirmed that mortality among populations with high educational attainment and adult groups continued to show solid positive associations with GDP per capita, urbanization index, and the Combined Variable, reinforcing the hypothesis of superior diagnostic capacity and comprehensive mortality reporting in wealthier metropolitan hubs.

Conversely, the inverse associations observed among highly vulnerable groups, such as populations with no formal instruction and the brown population, with municipal GDP persisted in the spatial model. This confirms that structural poverty, lack of infrastructure, and severe underreporting are deep-rooted territorial realities in Brazil, independent of spatial autocorrelation. Ultimately, integrating exploratory correlations with spatial econometrics provides a comprehensive, highly robust visualization of how structural and environmental inequalities drive respiratory mortality across the country.

## 5. Conclusions

This study demonstrated the importance of spatial analysis as a strategic tool for understanding the geographic distribution of mortality from respiratory diseases in Brazil. It revealed how socioeconomic, environmental, and demographic factors shape vulnerability patterns in different regions of the country. The application of geostatistical methods identified persistent spatial clusters and revealed relevant correlations between explanatory variables and health outcomes, highlighting structural inequalities that persist over time.

It is worth noting that, based on the correlation analyses presented, the study enabled the selection of municipalities for an integrated database. Subsequently, it may support complementary analyses using deep learning techniques to investigate correlation patterns associated with socioeconomic and environmental variables.

The North and Northeast regions showed greater vulnerability, as evidenced by negative correlations between mortality and indicators of GDP per capita, education, and the urbanization index. These patterns reflect historical limitations in access to healthcare services and basic infrastructure. In contrast, in the South and Southeast regions, the effects of intense urbanization and exposure to air pollutants, such as $CO_2$ and $N_2O$, were more pronounced, indicating that environmental determinants also play an important role in mortality.

The results reinforce the need for integrated, territorially oriented public policies that align the actions of the Unified Health System (SUS) with intersectoral strategies to tackle social and environmental inequalities. Such strategies include strengthening health surveillance, targeted prevention campaigns, and adaptive response protocols for critical events related to pollution and climate change.

By providing robust empirical evidence on the interactions between health, environment, and socioeconomic inequalities, this study contributes to advancing policies aligned with SDG 3 (Good Health and Well-Being), SDG 10 (Reduced Inequalities), and SDG 13 (Climate Action). Integrating these agendas is essential to promote environmental justice and health equity, especially in contexts marked by historical vulnerabilities and territorial heterogeneity.

Finally, it is important to acknowledge methodological limitations in calculating epidemiological indicators. Unlike studies that employ empirical Bayesian smoothing to adjust for population variance (Silva et al., 2014), we utilized crude mortality rates per 100,000 inhabitants. While this standardizes the metrics to account for absolute demographic size differences across municipalities, rates in towns with very small populations or within highly specific demographic subgroups may exhibit statistical instability due to the law of small numbers. Future studies could benefit from incorporating Bayesian spatial models to smooth these estimates and further refine the identification of risk clusters.

Furthermore, the strict application of a spatial contiguity matrix required the exclusion of insular municipalities lacking land borders, such as Fernando de Noronha and Ilha Bela. While alternative spatial weightings based on Euclidean distance could mathematically incorporate these areas, such an approach would force artificial spatial linkages over large oceanic distances, ignoring the reality that true

epidemiological and environmental continuity relies on shared borders and immediate commuting flows. Nonetheless, the contiguity model's inability to assess the spatial vulnerability of these isolated island populations remains a methodological limitation of the study design.

In addition, the composite metric (Combined Variable) aggregated normalized variables via an unweighted sum. While useful for exploratory dimensionality reduction, this approach assumes equal weights and linear additive effects, which may imply simplifications in representing complex socioeconomic and demographic interactions compared to empirically weighted models (such as PCA). Nevertheless, this study represents a comprehensive initial effort to apply spatial autocorrelation techniques to respiratory disease mortality at the municipal level across Brazil, providing a robust foundation for future, more complex modeling.

**Authors' Contributions:** NICOMEDES, N.P.: contributed to the conception and design of the study, acquisition of data, analysis and interpretation of data, and drafting of the article; CAMARGO, P.C.M.G.: contributed to the analysis and interpretation of data. Liliane contributed to data acquisition, analysis and interpretation of data; ARENAS, L.A.O.: contributed to the critical review of important intellectual content; LUSQUINO-FILHO, L.A.D.: contributed to the critical review of important intellectual content; SILVA, D.C.C.: contributed to the critical review of important intellectual content. All authors gave final approval of the version to be published.

**Conflicts of Interest:** There are no conflicts of interest or financial disclosures to declare by the authors.

**Ethics Approval:** Not applicable.

**Acknowledgments:** This study was funded by the Coordination for the Improvement of Higher Education Personnel (CAPES) under Grant number 001, and National Council for Scientific and Technological Development (CNPq) under Grant number 444734/2023-6.

**References**

ANUNCIAÇÃO, D. et al. Ways and detours in guarantee of health for the black population and the confrontation of racism in Brazil. *Ciência & Saúde Coletiva*. 2022, **27**(10), 3861–3870. https://doi.org/10.1590/1413-812320222710.08212022EN

ANSELIN, L. *Spatial Econometrics: Methods and Models*. Dordrecht: Kluwer Academic Publishers. 1988.

ANSELIN, L. Spatial externalities, spatial multipliers, and spatial econometrics. *International Regional Science Review.* 2003, **26**(2), 153-166. https://doi.org/10.1177/0160017602250972

ARRUDA, N.M., MAIA, A.G., ALVES, L.C. Desigualdade no acesso à saúde entre as áreas urbanas e rurais do Brasil: uma decomposição de fatores entre 1998 a 2008. *Cadernos de Saúde Pública***.** 2018, **34**(6), e00213816. https://doi.org/10.1590/0102-311X00213816

AYRES, J.G. et al. Climate change and respiratory disease: European Respiratory Society position statement. *European Respiratory Journal*. 2009, **34**(2), 295-302. https://doi.org/10.1183/09031936.00003409

BAQUI, P. et al. Comparing COVID-19 risk factors in Brazil using machine learning: the importance of socioeconomic, demographic and structural factors. *Scientific Reports*. 2021, **11**(1). https://doi.org/10.1038/s41598-021-95004-8

BRASIL. *Law No 12.187, of December 29, 2009*. Brasília: Presidency of the Republic, 2009. Available from: https://www.planalto.gov.br/ccivil_03/_ato2007-2010/2009/lei/l12187.htm

BRASIL. Ministry of Health. Brasil firma acordo com São Tomé e Príncipe para fortalecimento mútuo de sistemas de saúde. Available from: https://www.gov.br/saude/pt-br/assuntos/noticias/2025/marco/brasil-firma-acordo-com-sao-tome-e-principe-para-fortalecimento-mutuo-de-sistemas-de-saude

BRASIL. Ministry of Health. Dia Mundial sem Tabaco: Brasil tem redução no número de fumantes. Available from: https://www.gov.br/saude/pt-br/assuntos/noticias/2021/junho/dia-mundial-sem-tabaco-brasil-tem-reducao-no-numero-de-fumantes

BRASIL. Ministry of the Environment and Climate Change. *NDC - ambição climática do Brasil, 3ª atualização - 2023*. Available from: https://www.gov.br/mma/pt-br/assuntos/mudanca-do-clima/NDC

BUSTAMANTE, M.M.C. et al. Estimating greenhouse gas emissions from cattle raising in Brazil. *Climatic Change*. 2012, **115**(3-4), 559–577. https://doi.org/10.1007/s10584-012-0443-3

CÂMARA, G. et al. Análise Espacial e Geoprocessamento. In: S. DRUCK, M.S. CARVALHO, G. CÂMARA and A.V.M. MONTEIRO, eds. *Análise Espacial de Dados Geográficos*, Brasília: EMBRAPA, 2004, pp. 21-54.

CAVALCANTE, T.M. et al. Brazil: balance of the National Tobacco Control Policy in the last decade and dilemmas. *Cadernos de Saúde Pública*. 2017, **33**, e00138315. https://doi.org/10.1590/0102-311X00138315

CHAVES, A.R.T. Vista do Trajetória da industrialização brasileira e suas diferenças regionais. *DRPEES*. 2022, **1**(1), 1–23. Available from: https://ojs.unialfa.com.br/index.php/desenvolvimentoregional/article/view/42

CONFALONIERI, U E.C. and MARINHO, D.P. Mudança climática global e saúde: perspectivas para o Brasil. *Revista Multiciência*. 2007, **8**, 48-64. Available from: https://cetesb.sp.gov.br/aguasinteriores/wp-content/uploads/sites/36/2014/05/confalonieri_mc_global_saude.pdf

CRIPPA, M., GUIZZARDI, D., PAGANI, F. et al. GHG emissions of all world countries. *Publications Office of the European Union*, Luxembourg. 2024. https://doi.org/10.2760/4002897

DILGER, M. et al. Distributions for time, interspecies and intraspecies extrapolation for deriving occupational exposure limits. *Journal of Applied Toxicology*. 2022, **42**(5), 898-912. https://doi.org/10.1002/jat.4305

DU, M. et al. Mutual associations of healthy behaviours and socioeconomic status with respiratory diseases mortality: a large prospective cohort study. *Nutrients*. 2023, **15**(8), 1872. https://doi.org/10.3390/nu15081872

EDEBELI, J., SPIRIG, C., ANET, J. Downscaling EDGAR emissions to local emission sectors for Switzerland. In: EGU General Assembly Conference Abstracts EGU21-8208. 2021.

GAFFNEY, A.W. et al. Socioeconomic inequality in respiratory health in the US from 1959 to 2018. *JAMA Internal Medicine*. 2021, **181**(7), 968-976. https://doi.org/10.1001/jamainternmed.2021.2441

GOMES, G. et al. Análise temporal da autocorrelação espacial de melanoma maligno da pele nas regiões Sul e Sudeste do Brasil. *Entorno Geografico*, 2025, 30, e20114692. https://doi.org/10.25100/eg.v0i30.14692

IBGE. INSTITUTO BRASILEIRO DE GEOGRAFIA E ESTATÍSTICA.
*Censo Demográfiaco 2022 - Favelas e Comunidades Urbanas: Resultados do universo*. Rio de Janeiro: IBGE, 2024a. Available from: https://biblioteca.ibge.gov.br/index.php/biblioteca-catalogo?view=detalhes&id=2102134

IBGE. INSTITUTO BRASILEIRO DE GEOGRAFIA E ESTATÍSTICA.
*Panorama do Censo 2022*. 2024b. Available from: https://censo2022.ibge.gov.br/panorama/

IPCC. *AR6 Synthesis Report Climate Change 2023*. S.l.: IPCC, 2023.
Available from: https://www.ipcc.ch/report/ar6/syr/

KAMENS, R.M. and STERN, A.C. Methane in air quality and automobile exhaust emission standards. *Journal of the Air Pollution Control Association*. 1973, **23**(7), 592-596. https://doi.org/10.1080/00022470.1973.10469812

KLEINBECK, S. and WOLKOFF, P. Exposure limits for indoor volatile substances concerning the general population: The role of population-based differences in sensory irritation of the eyes and airways for assessment factors. *Archives of Toxicology*. 2024, **98**(3), 617-662. https://doi.org/10.1007/s00204-023-03642-w

LESAGE, J. and PACE, R. K. *Introduction to Spatial Econometrics.* Boca Raton: CRC Press. 2009.

LOCATELLI, J.L. et al. A comprehensive assessment of greenhouse gas emissions research in the Cerrado region, Brazil. *CATENA*. 2024, **247**, 108538. https://doi.org/10.1016/j.catena.2024.108538

MAPBIOMAS. *Coleção 08*. 2024. Available from: https://brasil.mapbiomas.org/colecoes-mapbiomas/

MCCUTCHEON, K et al. Climate Change and Cardiovascular Disease in Africa. *Wits Journal of Clinical Medicine*. 2022, **4**(3), 135. Available from: https://hdl.handle.net/10520/ejc-wjcm_v4_n3_a3

MENON, J.M.L et al. A health-based recommended occupational exposure limit for nitrous oxide using experimental animal data based on a systematic review and dose-response analysis. *Environmental research*. 2021, **201**, 111575. https://doi.org/10.1016/j.envres.2021.111575

NASCIMENTO, B.R. et al. Trends in prevalence, mortality, and morbidity associated with high systolic blood pressure in Brazil from 1990 to 2017: estimates from the "Global Burden of Disease 2017" (GBD 2017) study. *Population Health Metrics*. 2020, **18**, 17. https://doi.org/10.1186/s12963-020-00218-z

NERI, M. and SOARES, W. Desigualdade social e saúde no Brasil. *Cadernos de saúde pública*. 2002, **18**, S77-S87. Available from: https://www.scielosp.org/article/ssm/content/raw/?resource_ssm_path=/media/assets/csp/v18s0/13795.pdf

NERY, L. M. et al. Analysis of models to estimate morbidity rates of respiratory diseases through deep learning. *Tropical Medicine & International Health*,2026, 31. https://doi.org/10.1111/tmi.70126

OLIVEIRA, P.P.V. et al. Indicadores referentes à cessação do comportamento de fumar no Brasil, Pesquisa Nacional de Saúde, edições 2013 e 2019. *Epidemiologia e Serviços de Saúde*. 2022, **31**, e2021388. https://doi.org/10.1590/SS2237-9622202200005.especial

ONU. *Transformando Nosso Mundo: a Agenda 2030 para o Desenvolvimento Sustentável*. Brasília: Presidência da República, 2015. Available from: https://brasil.un.org/pt-br/91863-agenda-2030-para-o-desenvolvimento-sustentavel

RAZAFINDRAKOTO, M. et al. Municípios in the Time of Covid-19 in Brazil: Socioeconomic Vulnerabilities, Transmission Factors and Public Policies. *The European Journal of Development Research*. 2021, **34**(6). https://doi.org/10.1057/s41287-021-00487-w

SATISH, U. et al. Is CO2 an indoor pollutant? Direct effects of low-to-moderate CO2 concentrations on human decision-making performance. *Environmental health perspectives*. 2012, **120**(12), 1671-1677. https://doi.org/10.1289/ehp.1104789

SILVA, D.C.C. et al. Análise da relação entre a distribuição espacial das morbidades por obesidade e hipertensão arterial para o estado de São Paulo, Brasil, de 2000 a 2010. *Ciência & Saúde Coletiva*. 2014*,* **19**(6), 1709–1719. https://doi.org/10.1590/1413-81232014196.15002013

WETZEL, S. et al. Changing socioeconomic and geographic gradients in cardiovascular disease risk factors among Indians aged 15–49 years – evidence from nationally representative household surveys. *The Lancet Regional Health – Europe*. 2023, **12**, 100188–100188. https://doi.org/10.1016/j.lansea.2023.100188

YE, L., YUAN, Y., CHEN, Y., LI, H. Spatial Zoning of Carbon Dioxide Emissions at the Intra-City Level Based on Ring-Layer and Direction Model: A Case Study of Shenzhen, China. Land. 2025, **14**(9):1714. https://doi.org/10.3390/land14091714